lubricants

MDPI

Article

Improvement of Mechanical Properties and Adhesion of Ti-Al-Si-N Coatings by Alloying with Ta

Artur R. Shugurov [1,2], Evgenii D. Kuzminov [1], Yuriy A. Garanin [1,2], Alexey V. Panin [1,2] and Andrey I. Dmitriev [1,3,*]

[1] Institute of Strength Physics and Material Science, Siberian Branch of the Russian Academy of Science, Akademicheskii pr. 2/4, 634055 Tomsk, Russia
[2] School of Nuclear Science & Engineering, National Research Tomsk Polytechnic University, 634050 Tomsk, Russia
[3] Department of Metal Physics, National Research Tomsk State University, 634050 Tomsk, Russia
* Correspondence: dmitr@ispms.ru

Abstract: The effect of the Ta content on the structure, mechanical properties and adhesion of magnetron-sputtered $Ti_{1-x-y-z}Al_xTa_ySi_zN$ coatings was studied. According to the energy-dispersive X-ray spectroscopy analysis, the coatings studied had the following chemical compositions: $Ti_{0.41}Al_{0.49}Si_{0.10}N$, $Ti_{0.38}Al_{0.47}Ta_{0.05}Si_{0.10}N$, $Ti_{0.36}Al_{0.44}Ta_{0.10}Si_{0.10}N$ and $Ti_{0.35}Al_{0.40}Ta_{0.15}Si_{0.10}N$. The X-ray diffraction experiments revealed the B1-type fcc crystal structure of the coatings. The increasing Ta content was found to induce the texture evolution from (200) to (111), which was attributed to a significant increase in the residual compressive stress in the coatings. The hardness monotonically increased from 32.7 to 42.2 GPa with increasing the Ta content, while the reduced Young's modulus decreased from 369 to 353 GPa. The adhesion of the coatings to the Ti substrate was evaluated by scratch testing. It was found that the $Ti_{0.36}Al_{0.44}Ta_{0.10}Si_{0.10}N$ coating was characterized by maximum adhesion strength, while incorporation of a larger amount of Ta resulted in earlier coating spallation due to the high residual compressive stress.

Keywords: Ti-Al-Ta-Si-N coatings; titanium; hardness; adhesion; scratching

Citation: Shugurov, A.R.; Kuzminov, E.D.; Garanin, Y.A.; Panin, A.V.; Dmitriev, A.I. Improvement of Mechanical Properties and Adhesion of Ti-Al-Si-N Coatings by Alloying with Ta. *Lubricants* **2022**, *10*, 178. https://doi.org/10.3390/lubricants10080178

Received: 8 July 2022
Accepted: 5 August 2022
Published: 7 August 2022

1. Introduction

In the past decades $Ti_{1-x}Al_xN$ coatings was increasingly used in cutting tool applications, aircraft and marine industries, mechanical engineering, chemical industry, etc. to improve surface hardness and resistance against oxidation, corrosion, erosion and wear of different tools and components [1–3]. The extensive use of the $Ti_{1-x}Al_xN$ coatings stems from their superior mechanical, tribological and thermal properties compared with binary nitrides such as TiN [1,4–7]. The enhanced hardness and wear resistance of the coatings result from non-equilibrium conditions of their deposition, which lead to the formation of an oversaturated $Ti_{1-x}Al_xN$ solid solution, where Al substitutes Ti in the TiN lattice, forming a metastable fcc NaCl structure [8,9]. The latter results in elastic distortions of the crystal lattice and, consequently, in solid solution hardening of the coatings [4]. At high Al contents ($x > 0.33$) grain boundary hardening and precipitation hardening also contribute to the increase in hardness, which can reach ~40 GPa at $x \approx 0.5$–0.6 [1,4,10]. Moreover, the hardness can be additionally increased by annealing at temperatures of 800–950 °C due to spinodal decomposition of the metastable $Ti_{1-x}Al_xN$ solid solution into domains enriched with TiN and cubic AlN (c-AlN) [7,11]. However, at higher temperatures and/or long thermal exposure the c-AlN domains transform into the stable hexagonal wurtzite (w-AlN) phase that induces a sharp decrease in the hardness and wear resistance of the coatings [1,12]. The $Ti_{1-x}Al_xN$ coatings also exhibit excellent oxidation resistance at temperatures up to 800–850 °C due to the formation of a dense outermost Al_2O_3 layer, which strongly suppresses the inward diffusion of oxygen [10,13,14]. At higher temperatures

the rapid formation of the bilayer oxide scale, which along with the dense top Al-rich layer contains the underlying porous Ti-rich layer, significantly deteriorates the oxidation resistance of the $Ti_{1-x}Al_xN$ coatings.

Numerous studies have revealed that further improvement of the mechanical and tribological performance, thermal stability and oxidation resistance of the $Ti_{1-x}Al_xN$ coatings can be achieved by alloying with Si [15–22]. Due to the limited solubility in Ti-Al-N, a small amount of Si atoms incorporates into the fcc crystal lattice substituting Ti and Al, while at the higher Si contents most of Si segregates at the Ti-Al-N grain boundaries [15,21,23]. In the latter case, the SiN_x tissue phase is formed in the $Ti_{1-x-y}Al_xSi_yN$ coatings, which impedes the growth of the Ti-Al-N grains, resulting in the microstructure comprised of the Ti-Al-N nanocrystallites embedded in the amorphous SiN_x matrix. The combined effect of the grain refinement and hindered dislocation motion owing to a large number of grain boundaries with increased cohesive strength due to the presence of the SiN_x tissue phase provides superhardness (>40 GPa) of such nanocomposite coatings [5,24]. Depending on the Ti/Al ratio and deposition conditions, the optimum Si content of the $Ti_{1-x-y}Al_xSi_yN$ coatings, can vary from ~2 to ~9 at.% (z = 0.04–0.18) [22]. At higher Si contents the hardness drastically drops, since the blocking effect of grain boundaries becomes insignificant because of too thick intergranular tissue phase. Alloying with Si decreases the friction coefficient and improves the wear resistance of the coatings due to the formation of SiO_2 and $Si(OH)_2$ tribolayers [22,25]. Si-alloying is also beneficial under water lubrication due to the formation of silica gel originating from the hydration of silicon [26]. The amorphous SiN_x tissue phase also hinders the spinodal decomposition of the Ti-Al-N nanocrystallites that improves the thermal stability of the coatings so that their high hardness can be retained up to 1100 °C [21,23]. The improved oxidation resistance of the $Ti_{1-x-y}Al_xSi_yN$ coatings is concerned with (i) the protective effect of the SiN_x tissue phase, which acts as a barrier for oxygen diffusion; (ii) the suppression of the anatase-to-rutile phase transformation that reduces crack generation in the oxide scale; (iii) the promoting effect of Si on the formation of a protective uppermost Al_2O_3 layer [20,27–29]. However, the $Ti_{1-x-y}Al_xSi_yN$ coatings are often characterized by low toughness [30–32] and poor adhesion to a substrate [18,30,33–35], which significantly restrict their potential application for the protection of different materials against erosion and wear. Therefore, it is of crucial importance to improve the wear resistance of the coatings, especially for the applications using soft metal substrates, since insufficient load-bearing capacity of the coating/substrate system results in large bending deformation of the coating, which can induce its catastrophic failure [36].

Two main strategies have been proposed to enhance the toughness and adhesion of the $Ti_{1-x-y}Al_xSi_yN$ coatings, which assume the design of their multilayer architecture, consisting of alternating $Ti_{1-x-y}Al_xSi_yN$ and other ceramic or metal layers [30–32,34], and the elaboration of coatings with out-of-plane Si gradient distribution, which allows eliminating of the sharp interface between the coating and substrate [35]. One more approach to improve the performance of the $Ti_{1-x-y}Al_xSi_yN$ coatings is their alloying with an additional chemical element [37]. In particular, addition of Ta to the $Ti_{1-x}Al_xN$ solid solution has been shown to provide increased toughness with retaining high hardness [38–40]. Recent analysis of the electronic structure of Ti-Al-Ta-N solid solutions by ab-initio calculations have showed that the increase in their toughness is concerned with growing metallicity of interatomic bonds caused by Ta alloying [41]. In addition, the $Ti_{1-x-y}Al_xTa_yN$ coatings exhibited significantly higher thermal stability (up to 1200 °C) and oxidation resistance than the $Ti_{1-x}Al_xN$ coatings. The enhanced thermal stability has been explained by changes in the electronic structure caused by incorporation of Ta atoms into the crystal lattice and by higher diffusion activation energy for Ta compared to Ti and Al [42]. The improved oxidation resistance has been attributed to a decrease in the amount of oxygen vacancies in the oxide layer and to suppression of the anatase-rutile phase transformation in the TiO_2 layer [43,44]. More recently it has been found that alloying with Ta also significantly enhances adhesion of $Ti_{1-x}Al_xN$ coatings to a titanium substrate [45]. However, the effect of Ta alloying on the adhesion of the $Ti_{1-x-y}Al_xSi_yN$ coatings has not yet been investigated.

Therefore, this study is focused on the investigation of structure, mechanical properties and adhesion of the $Ti_{1-x-y-z}Al_xTa_ySi_zN$ coatings.

2. Materials and Methods

The $Ti_{1-x-y-z}Al_xTa_ySi_zN$ coatings were deposited on stationary titanium substrates (10 mm × 10 mm × 2 mm) by DC magnetron sputtering. The Ti substrates were preliminary mechanically polished and ultrasonically cleaned in rectified alcohol. In addition, the same coatings were deposited on Si (100) substrates to perform the examination of fracture cross-sections and the measurement of the residual stress. Prior to the deposition, all the substrates were sputter-cleaned with Ar^+ ions for 20 min. Then a 50 nm thick TiAl layer was deposited to improve coating adhesion. The Ta-free coatings were sputtered using a compound TiAl (55/45 at.%) target 125 mm in diameter with Si inserts. The deposition of the Ta-alloyed coatings was performed by co-sputtering using the Ti/Al/Si target and a Ta (99.99%) target 100 mm in diameter. The magnetrons were tilted at an angle of 100° between the magnetron axes. The distances from the center of the substrate holder to the centers of the targets were 90 mm. The Ta content in the coatings was changed by varying the power density at the Ta target from 3.8 to 6.2 W/cm^2, while the power density at the Ti/Al/Si target was kept constant at 11.4 W/cm^2. The Si content in the coatings was maintained at 5 at.% (z = 0.1) by varying the number of the Si inserts. The sputtering was carried out in an Ar + N_2 gas mixture at a constant pressure of 0.3 Pa with a nitrogen partial pressure of 0.06 Pa. The 3.0 μm thick coatings were deposited on grounded substrates heated to 425 °C.

The determination of the chemical composition of the coatings by energy-dispersive X-ray spectroscopy (EDS) and the investigation of the microstructure of their fracture cross-sections were performed using a LEO EVO 50 scanning electron microscope (SEM, Carl Zeiss, Jena, Germany). The phase composition of the coatings was investigated by X-ray diffraction (XRD) in the Bragg-Brentano configuration using an XRD-7000 diffractometer (Shimadzu, Kyoto, Japan, the equipment of the Center for sharing use "Nanomaterials and nanotechnologies" of Tomsk Polytechnic University supported by the RF Ministry of Education and Science, project No. 075-15-2021-710). CuKα radiation with a wavelength of λ = 1.5406 Å was used. The texture coefficients were calculated from XRD patterns, using following equation [46]:

$$TC_{hkl} = \frac{I_{hkl}/I_{0hkl}}{\frac{1}{n}\sum_n \left(I_{hkl}/I_{0hkl}\right)} \quad (1)$$

where I_{hkl} is the measured intensity of the XRD peak corresponding to the (hkl) plane for the phase; I_{ohkl} is the intensity of the same XRD peak of a standard reference sample; n is the number of analyzed XRD peaks. The residual stresses σ were extracted from substrate curvature measurements performed with an Alpha-Step IQ surface profiler (KLA-Tencor, San Jose, CA, USA), using the Stoney equation [47]. Nanoindentation measurements were carried out with a NanoTest system (Micro Materials Ltd., UK) using a Berkovich indenter in the load-controlled mode. The loading and unloading times were set at 20 s with 10 s dwell time at the maximum load and 60 s dwell time at 90% unloading for thermal drift correction. The maximum applied load was set at 20 mN to ensure penetration depths below 10% of the coating thickness in order to exclude the substrate effect on the measured mechanical characteristics. 20 indents were made for each coating, and the results obtained were averaged. The hardness (H) and Young's modulus (E) of the coatings were determined from load vs. displacement curves using the Oliver-Pharr method [48]. The coating adhesion was evaluated by scratch testing using a Revetest instrument (CSM instruments, Peseux, Switzerland) with a conical Rockwell stylus, which had a tip curvature radius of 200 μm. The scratches were made 7 mm long with a sliding speed of 2 mm/min and an increasing applied load. The maximum applied load was 55 N. The failure events and the corresponding critical loads were detected from the variations of the friction coefficient and acoustic emission signals as well as the microscopic examination of the scratch grooves with an Axiovert 40 Mat optical microscope (Carl Zeiss, Jena, Germany).

3. Results

An EDS analysis showed that the coatings studied have the following chemical compositions: $Ti_{0.41}Al_{0.49}Si_{0.10}N$, $Ti_{0.38}Al_{0.47}Ta_{0.05}Si_{0.10}N$, $Ti_{0.36}Al_{0.44}Ta_{0.10}Si_{0.10}N$ and $Ti_{0.35}Al_{0.40}Ta_{0.15}Si_{0.10}N$. Since the Si content in the coatings was maintained constant by addition of the Si inserts to the Ti/Al/Si target, the increase in the Ta content resulted in the decrease of the Ti and Al contents. It should also be noted the increase in the Ti/Al ratio with increasing Ta content from 0.05 to 0.15, which can be attributed to scattering of light Al atoms due to collisions with heavy Ta atoms.

Figure 1 displays the XRD patterns of the coatings, which show their B1-type fcc crystal structure. There is no indication of the presence of other crystalline phases, in particular wurtzite, which significantly deteriorates hardness of Ti-Al-N-based coatings. The w-AlN phase is often observed in $Ti_{1-x-y}Al_xSi_yN$ coatings because of the promoting effect of Si on its formation [27,30,49,50]. The absence of w-AlN in the $Ti_{1-x-y-z}Al_xTa_ySi_zN$ coatings is evidently concerned with the fact that even in the $Ti_{0.41}Al_{0.49}Si_{0.10}N$ coating with the highest (Al + Si) content the (Al + Si)/(Ti + Al + Si) ratio is equal to 0.59, whereas the w-AlN phase has been reported to form at (Al + Si)/(Ti + Al + Si) = 0.61 [30,49]. It can be seen from Figure 1 that the increase in the Ta content results in shifting of the XRD peaks to lower diffraction angles that is due to the increasing lattice constant. As shown in Figure 2, the lattice constant deduced from the XRD patterns demonstrates a virtually linear increase from 0.4234 nm in $Ti_{0.41}Al_{0.49}Si_{0.10}N$ to 0.4255 nm in $Ti_{0.35}Al_{0.40}Ta_{0.15}Si_{0.10}N$, which can be attributed to the incorporation of large Ta atoms in the crystal lattice as well as an increase in a residual compressive stress in the coatings. The latter is in good agreement with the results of the substrate curvature measurements, which are presented in Figure 3. It can be seen that all the coatings are characterized by compressive residual stresses, which increase with the Ta content, reaching –6.8 GPa in $Ti_{0.35}Al_{0.40}Ta_{0.15}Si_{0.10}N$.

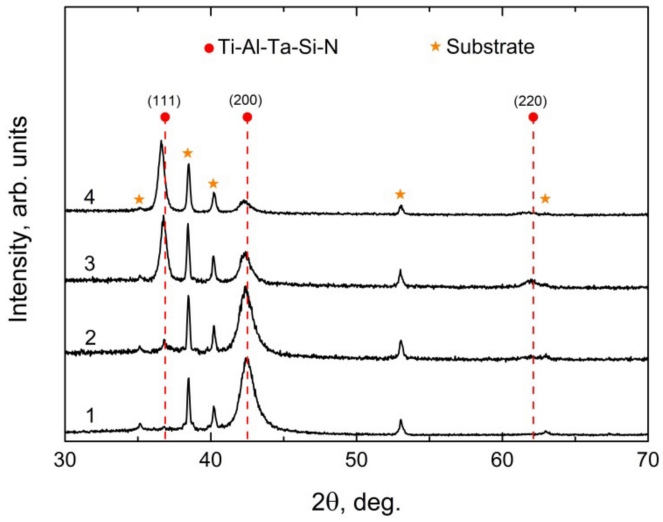

Figure 1. X-ray diffraction patterns of $Ti_{0.41}Al_{0.49}Si_{0.10}N$ (1), $Ti_{0.38}Al_{0.47}Ta_{0.05}Si_{0.10}N$ (2), $Ti_{0.36}Al_{0.44}Ta_{0.10}Si_{0.10}N$ (3) and $Ti_{0.35}Al_{0.40}Ta_{0.15}Si_{0.10}N$ (4) coatings.

The Ti-Al-Ta-Si-N peaks demonstrate significant broadening, which can be ascribed to high microstrains caused by elastic distortions of the TiN crystal lattice due to the incorporation of Al, Ta and Si, as well as, a small grain size in the coatings. Indeed, as shown in Figure 4, the average grain sizes in the $Ti_{1-x-y-z}Al_xTa_ySi_zN$ coatings calculated using the Debye-Scherrer equation [51] do not exceed 12 nm. A slight increase in the average grain size is observed at the higher Ta contents. It should also be noted the effect of the Ta content on the preferred orientation of grains in the $Ti_{1-x-y-z}Al_xTa_ySi_zN$ coatings. It is seen from Figure 1 that the $Ti_{0.41}Al_{0.49}Si_{0.10}N$ coating has a strong (200) texture, while with increasing the Ta content the relative intensity of the (200) peak decreases and the intensity of the (111) peak grows. As a result, the $Ti_{0.35}Al_{0.40}Ta_{0.15}Si_{0.10}N$ coating is characterized

by the (111) preferred orientation. This texture evolution is clearly observed in Figure 5, which presents the texture coefficients (*TC*) of the coatings for the (111) and (200) crystal planes as a function of the Ta content. It can be seen that *TC* of the (111) plane increases with an increase in *y*, while the texture coefficient of the (200) plane exhibits the opposite behavior. It is known that high strains (stresses) favor the (111) texture to form in TiN-based coatings, because this crystallographic orientation is characterized by the lowest Young's modulus [52,53]. Therefore, it can be thought that the increasing residual compressive stress in the $Ti_{1-x-y-z}Al_xTa_ySi_zN$ coatings is responsible for their texture evolution.

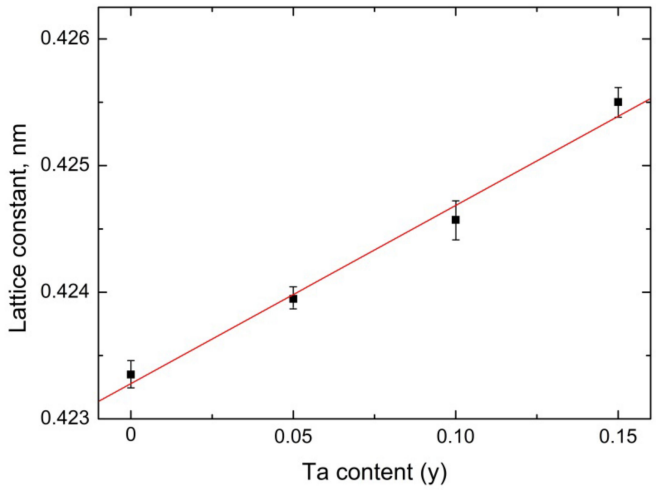

Figure 2. Lattice constant of the $Ti_{1-x-y-z}Al_xTa_ySi_zN$ coatings as a function of the Ta content.

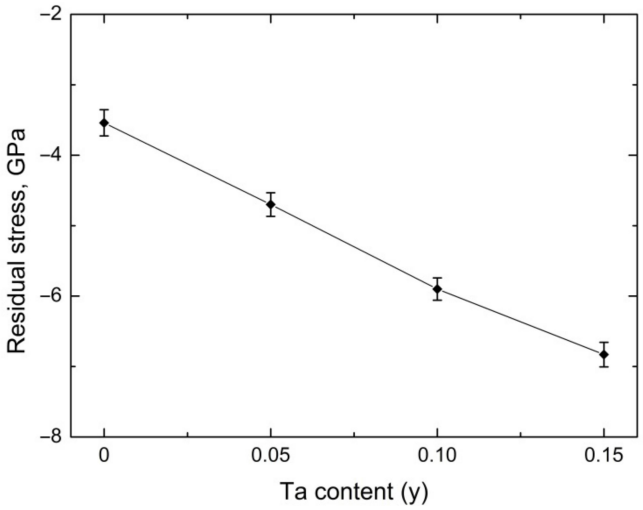

Figure 3. Residual stress in the $Ti_{1-x-y-z}Al_xTa_ySi_zN$ coatings as a function of the Ta content.

The fracture cross-section morphology of the coatings is shown in Figure 6. It is visible that the coatings are characterized by the similar dense non-columnar fine-grained structure, which is in good agreement with the XRD results. No cracks, imperfections and delaminations are observed in the micrographs.

Figure 7a exhibits the hardness and reduced Young's modulus of the $Ti_{1-x-y-z}Al_xTa_ySi_zN$ coatings as a function of the Ta content. The hardness monotonically increases from 32.7 to 42.2 GPa with increasing *y*. Considering the similar microstructures and grain sizes of the coatings, the hardness increase can be attributed primarily to the increasing residual compressive stresses. This is clearly evidenced from Figure 7b, which shows that the hardness linearly increases with the compressive stress. The latter is in good agreement with the earlier studies, which have reported a linear relationship between the compressive stress and hardness in transition metal nitride coatings [54,55]. The reduced Young's modulus

demonstrates the opposite behavior, decreasing from 369 to 353 GPa. The same trend in the dependence of E^* on the Ta content has been observed earlier for $Ti_{1-x-y}Al_xTa_yN$ coatings [38,40]. It has been ascribed to significant changes in chemical bonding caused by Ta incorporation [38,41]. The opposite trends in H and E^* result in a monotonical increase in the (H/E^*) and H^3/E^{*2} ratios (see Figure 8), which are associated with the elastic [56] and plastic strain to failure [57], respectively. Since these ratios are commonly used to rank ductility and toughness of coatings [58], their observed behavior indicates the toughness enhancement of the $Ti_{1-x-y-z}Al_xTa_ySi_zN$ coatings with increasing the Ta content.

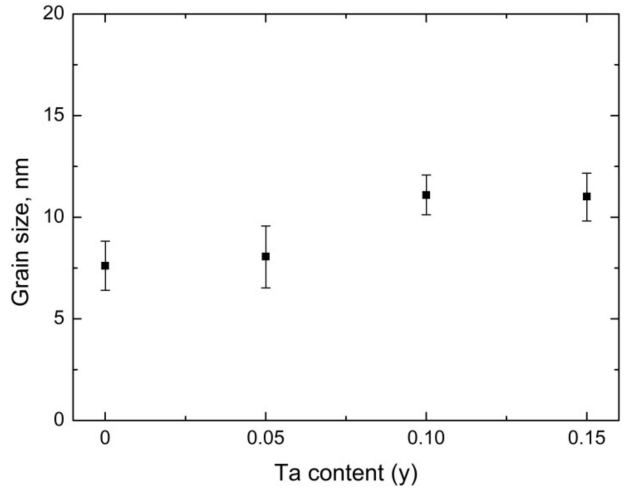

Figure 4. Average grain size in the $Ti_{1-x-y-z}Al_xTa_ySi_zN$ coatings as a function of the Ta content.

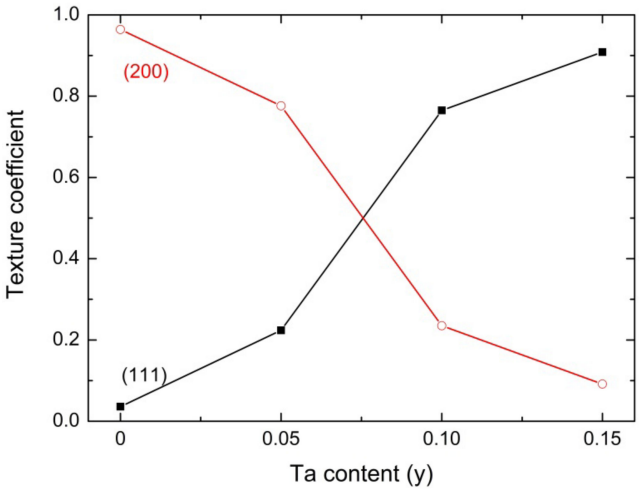

Figure 5. Texture coefficient of the $Ti_{1-x-y-z}Al_xTa_ySi_zN$ coatings as a function of the Ta content.

The adhesion strength of the $Ti_{1-x-y-z}Al_xTa_ySi_zN$ coatings was evaluated by the scratch testing. The results are presented in Figure 9, which illustrates the friction coefficient (μ) and acoustic emission signal (AE) as a function of the scratching distance and applied normal load. During the scratching, the stylus induced plastic ploughing of the soft Ti substrate, which resulted in the formation of the residual scratch grooves with pile-ups at their flanks. Microscopic examination of the grooves showed that the coating failure primarily occurred by the formation of forward semicircular conformal cracks propagated outwards from the grooves. This failure mode is often observed, when scratching hard coatings on soft substrates [59,60]. It is concerned with large compressive stresses ahead of the moving stylus, which cause a pile-up to form due to displacing the substrate material from the bottom of the groove. Due to the rigid bonding between the coating and substrate, the strain accommodation results in coating bending. The bending deformation generates

tensile stresses in the top layer of the coatings at the pile-ups, which lead to their cracking around the front half of the stylus with a semicircular pattern. The formation of first conformal cracks caused the first sudden peaks of acoustic emission to appear, which was used to correctly determine the first critical load L_{c1}. This load corresponds to the first crack event during scratching and characterizes coating cohesive strength. As can be seen from Figure 9, the L_{c1} load monotonically increases with the Ta content, so that it is ~1.7 times higher for $Ti_{0.35}Al_{0.40}Ta_{0.15}Si_{0.10}N$ than for $Ti_{0.41}Al_{0.49}Si_{0.10}N$. This behavior of L_{c1} can be attributed to an increase in the load bearing capacity of the coatings with higher y due to the enhanced hardness as well as to their improved toughness. The latter is confirmed by a good agreement between the observed increasing trend of L_{c1} and the variations of H/E^* and H^3/E^{*2} shown in Figure 8.

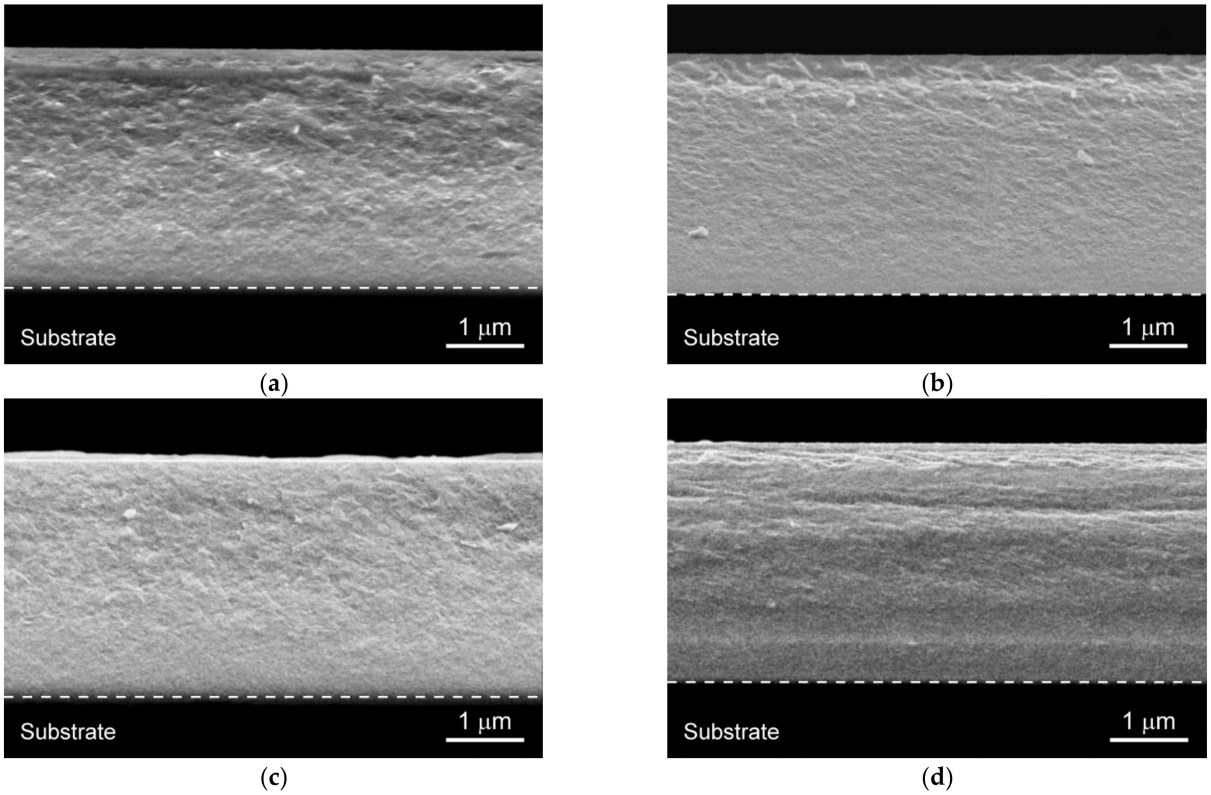

Figure 6. Cross-sectional SEM micrographs of (**a**) $Ti_{0.41}Al_{0.49}Si_{0.10}N$, (**b**) $Ti_{0.38}Al_{0.47}Ta_{0.05}Si_{0.10}N$, (**c**) $Ti_{0.36}Al_{0.44}Ta_{0.10}Si_{0.10}N$ and (**d**) $Ti_{0.35}Al_{0.40}Ta_{0.15}Si_{0.10}N$ coatings.

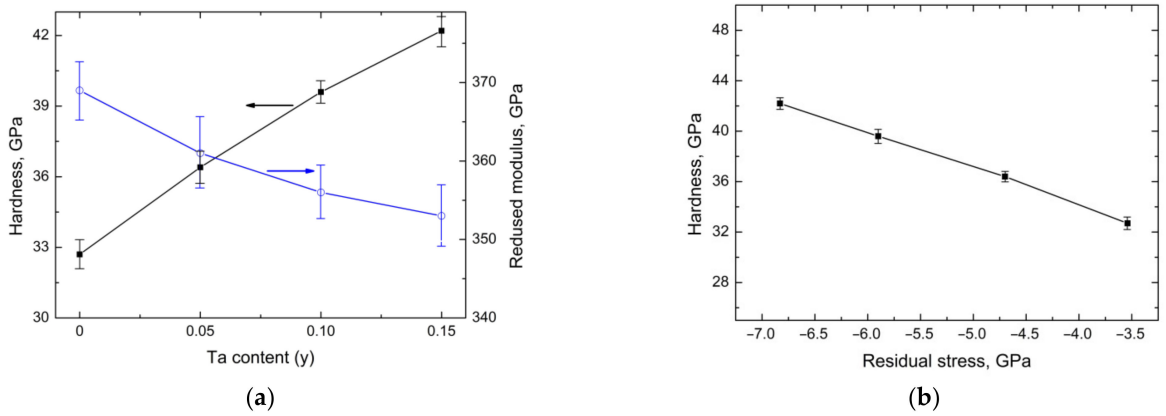

Figure 7. (**a**) The hardness and reduced Young's modulus of the $Ti_{1-x-y-z}Al_xTa_ySi_zN$ coatings as a function of the Ta content. (**b**) The hardness vs. residual compressive stress.

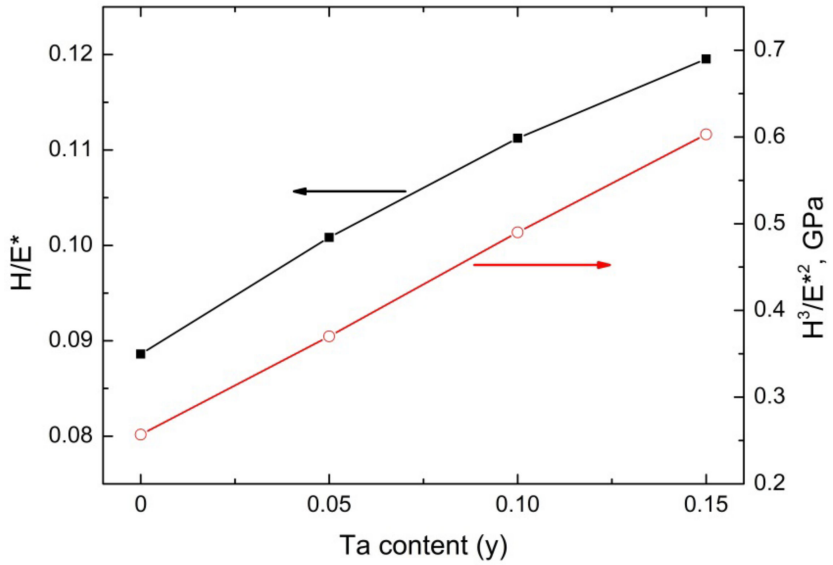

Figure 8. H/E * and H^3/E^{*2} ratios of the $Ti_{1-x-y-z}Al_xTa_ySi_zN$ coatings as a function of the Ta content.

The following increasing of the applied load eventually results in continuous spallation of the coatings in the scratch grooves. The onset of the continuous spallation, which is accompanied by increasing friction coefficient from ~0.2 to a value ~0.6 corresponding to the titanium substrate due to its exposure, defines the second critical load L_{c2}, which is adopted as a measure of interfacial adhesion strength. In contrast to the first critical load, L_{c2} initially increases with the Ta content and reaches a maximum value at $y = 0.10$ but then drops at $y = 0.15$. Thus, despite the monotonic toughening of the $Ti_{1-x-y-z}Al_xTa_ySi_zN$ coatings with increasing the Ta content, the $Ti_{0.35}Al_{0.40}Ta_{0.15}Si_{0.10}N$ coating was characterized by weaker adhesion.

Considering the above results, it can be thought that it is the high residual compressive stress, which is responsible for the poor adhesion strength of the $Ti_{0.35}Al_{0.40}Ta_{0.15}Si_{0.10}N$ coating. It is well-known, that the large compressive stresses ahead of the moving stylus can induce buckling delamination of the coating in local regions, where bonding between the coating and substrate is weakened by interfacial defects [59]. According to [61], the critical stress σ_b, which induces coating buckling of a region of size L is given by:

$$\sigma_b = C\left(\frac{h}{L}\right)^2 \frac{E}{1-\nu^2}, \quad (2)$$

where C is the constant, which depends on the buckling shape, h is the coating thickness, E and ν are the Young's modulus and Poisson's ratio of the coating, respectively. In the case of a planar interface, rather large regions of the coating debonding are usually needed to produce its buckling. However, it has been shown [62,63], that for a curved interface, which is formed in the pile-up area, the compressive in-plane stress σ_0 generates a tensile stress component normal to the interface, given by:

$$\sigma_t = \sigma_0 \frac{h}{R}, \quad (3)$$

where R is the radius of the local interface curvature. This stress component is a driving force for detachment and buckling of the coating in the pile-up area. After buckling, the stylus passes over this region and crushes the coating resulting in its spallation. This mechanism is obviously realized, when scratching the $Ti_{1-x-y-z}Al_xTa_ySi_zN$ coatings. Since the in-plane stress σ_0 is the sum of the stress introduced by the stylus and the residual stress, the higher residual stress provides coating spallation at a lower applied load. As a result, the L_{c2} load in the $Ti_{1-x-y-z}Al_xTa_ySi_zN$ coatings is governed by the competition

between the enhancement of their toughness and the increase of the residual compressive stress, which results in its peak value in $Ti_{0.36}Al_{0.44}Ta_{0.10}Si_{0.10}N$.

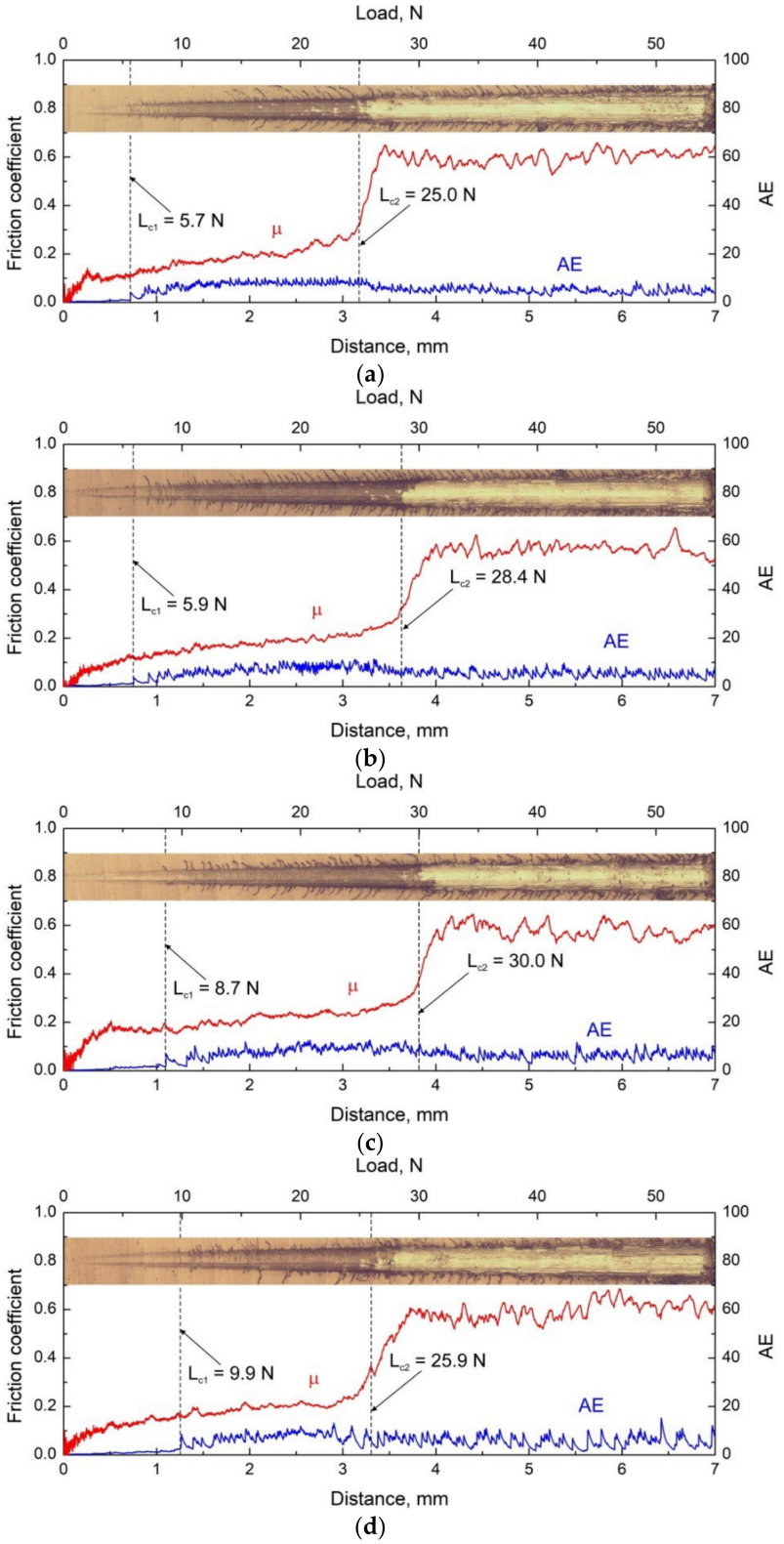

Figure 9. Scratch tracks, friction coefficients, acoustic emission signals and critical loads of the (**a**) $Ti_{0.41}Al_{0.49}Si_{0.10}N$, (**b**) $Ti_{0.38}Al_{0.47}Ta_{0.05}Si_{0.10}N$, (**c**) $Ti_{0.36}Al_{0.44}Ta_{0.10}Si_{0.10}N$ and (**d**) $Ti_{0.35}Al_{0.40}Ta_{0.15}Si_{0.10}N$ coatings.

4. Conclusions

The effect of the Ta content on the structure, mechanical properties and scratching behavior of $Ti_{1-x-y-z}Al_xTa_ySi_zN$ coatings was studied. The X-ray diffraction investigations showed that an increase in the Ta content from y = 0 to 0.15 resulted in the increasing lattice parameter and the change of the preferred orientation of crystallites from (200) to (111). It was found that the coatings were characterized by compressive residual stresses, which increased with the Ta content and reached –6.8 GPa in $Ti_{0.35}Al_{0.40}Ta_{0.15}Si_{0.10}N$. It was found significant hardening of the coatings with an increase in the Ta content (from 32.7 to 42.2 GPa), while their elastic modulus exhibited a decreasing trend. The scratch testing revealed a monotonic increase in the crack resistance of the $Ti_{1-x-y-z}Al_xTa_ySi_zN$ coatings with the increasing Ta content. At the same time, the maximum adhesion strength was found in the $Ti_{0.36}Al_{0.44}Ta_{0.10}Si_{0.10}N$ coating, while the further increasing of y up to 0.15 resulted in earlier coating spallation due to high residual compressive stress. Thus, alloying with Ta provided superior hardness, toughness and adhesion of the $Ti_{1-x-y-z}Al_xTa_ySi_zN$ coatings over the Ta-free coating with the same Si content.

Author Contributions: Conceptualization, A.R.S.; methodology, A.R.S.; investigation, E.D.K., A.R.S., A.V.P. and Y.A.G.; data curation, E.D.K. and Y.A.G.; writing—original draft preparation, A.R.S.; writing—review and editing, A.R.S., A.V.P. and A.I.D.; visualization, E.D.K.; supervision, A.I.D.; project administration, A.I.D.; funding acquisition, A.I.D. All authors have read and agreed to the published version of the manuscript.

Funding: This work was funded by the Russian Science Foundation, grant 22-19-00441.

Institutional Review Board Statement: Not applicable.

Informed Consent Statement: Not applicable.

Data Availability Statement: The data presented in this study are available on request from the corresponding author.

Acknowledgments: The investigations have been carried out using the equipment of Share Use Centre "Nanotech" of the ISPMS SB RAS.

Conflicts of Interest: The authors declare no conflict of interest.

References

1. PalDey, S.; Deevi, S.C. Single Layer and Multilayer Wear Resistant Coatings of (Ti,Al)N: A Review. *Mater. Sci. Eng. A* **2003**, *342*, 58–79. [CrossRef]
2. Zhao, J.; Liu, Z.; Wang, B.; Song, Q.; Ren, X.; Wan, Y. Effects of Al content in TiAlN coatings on tool wear and cutting temperature during dry machining IN718. *Tribol. Intern.* **2022**, *171*, 107540. [CrossRef]
3. Sousa, V.F.C.; da Silva, F.J.G.; Pinto, G.F.; Baptista, A.; Alexandre, R. Characteristics and Wear Mechanisms of TiAlN-based Coatings for Machining Applications: A Comprehensive Review. *Metals* **2021**, *11*, 260. [CrossRef]
4. Liu, Z.-J.; Shum, P.W.; Shen, Y.G. Hardening Mechanisms of Nanocrystalline Ti–Al–N Solid Solution Films. *Thin Solid Films* **2004**, *468*, 161–166. [CrossRef]
5. Çalişkan, H.; Panjan, P.; Paskvale, S. Monitoring of Wear Characteristics of TiN and TiAlN Coatings at Long Sliding Distances. *Tribol. Trans.* **2014**, *57*, 496–502. [CrossRef]
6. Shulepov, I.A.; Kashkarov, E.B.; Stepanov, I.B.; Syrtanov, M.S.; Sutygina, A.N.; Shanenkov, I.; Obrosov, A.; Weiß, S. The Formation of Composite Ti-Al-N Coatings Using Filtered Vacuum Arc Deposition with Separate Cathodes. *Metals* **2017**, *7*, 497. [CrossRef]
7. Chen, L.; Paulitsch, J.; Du, Y.; Mayrhofer, P.H. Thermal Stability and Oxidation Resistance of Ti-Al-N Coatings. *Surf. Coat. Technol.* **2012**, *206*, 2954–2960. [CrossRef]
8. Rogström, L.; Ullbrand, J.; Almer, J.; Hultman, L.; Jansson, B.; Odén, M. Strain Evolution during Spinodal Decomposition of TiAlN Thin Films. *Thin Solid Films* **2012**, *520*, 5542–5549. [CrossRef]
9. Shugurov, A.R.; Panin, A.V.; Dmitriev, A.I.; Nikonov, A.Y. Multiscale Fracture of Ti-Al-N Coatings under Uniaxial Tension. *Phys. Mesomech.* **2021**, *24*, 185–195. [CrossRef]
10. Zhou, M.; Makino, Y.; Nose, M.; Nogi, K. Phase Transition and Properties of Ti–Al–N Thin Films Prepared by r.f.-plasma Assisted Magnetron Sputtering. *Thin Solid Films* **1999**, *339*, 203–208. [CrossRef]
11. Mayrhofer, P.H.; Hultman, L.; Schneider, J.M.; Staron, P.; Clemens, H. Spinodal Decomposition of Cubic $Ti_{1-x}Al_xN$: Comparison between Experiments and Modeling. *Int. J. Mater. Res.* **2007**, *98*, 1054–1059. [CrossRef]

12. Rachbauer, R.; Massl, S.; Stergar, E.; Holec, D.; Kiener, D.; Keckes, J.; Patscheider, J.; Stiefel, M.; Leitner, H.; Mayrhofer, P.H. Decomposition Pathways in Age Hardening of Ti-Al-N Films. *J. Appl. Phys.* **2011**, *110*, 023515. [CrossRef]
13. McIntyre, D.; Greene, J.E.; Håkansson, G.; Sundgren, J.-E.; Münz, W.-D. Oxidation of Metastable Single-phase Polycrystalline $Ti_{0.5}Al_{0.5}N$ Films: Kinetics and Mechanisms. *J. Appl. Phys.* **1990**, *67*, 1542–1553. [CrossRef]
14. Chavee, L.; Serag, E.; da Silva Pires, M.; Lucas, S.; Haye, E. A mechanistic approach of oxidation resistance, structural and mechanical behaviour of TiAlN coatings. *Appl. Surf. Sci.* **2022**, *586*, 152851. [CrossRef]
15. Carvalho, S.; Rebouta, L.; Cavaleiro, A.; Rocha, L.A.; Gomes, J.; Alves, E. Microstructure and Mechanical Properties of Nanocomposite (Ti,Si,Al)N Coatings. *Thin Solid Films* **2001**, *398*, 391–396. [CrossRef]
16. Zhao, F.; Wang, L.; Wang, X. Microstructure and properties of TiAlSiN ultra-hard coatings prepared by plasma immersion ion implantation and deposition with TiAlSi alloy cathodes. *Vacuum* **2020**, *174*, 109194. [CrossRef]
17. Zhang, K.; Xin, L.; Ma, T.; Chang, H.; Lu, Y.; Feng, C.; Zhu, S.; Wange, F. Investigation of the role of silicon in TiAlSiN coating deposited on TiAl alloys during long-term oxidation. *Corros. Sci.* **2022**, *204*, 110394. [CrossRef]
18. Tillmann, W.; Dildrop, M. Influence of Si Content on Mechanical and Tribological Properties of TiAlSiN PVD Coatings at Elevated Temperatures. *Surf. Coat. Technol.* **2017**, *321*, 448–454. [CrossRef]
19. Pei, F.; Liu, H.J.; Chen, L.; Xu, Y.X.; Du, Y. Improved Properties of TiAlN Coating by Combined Si-Addition and Multilayer Architecture. *J. Alloys Compd.* **2019**, *790*, 909–916. [CrossRef]
20. Zhu, L.; Hu, M.; Ni, W.; Liu, Y. High Temperature Oxidation Behavior of $Ti_{0.5}Al_{0.5}N$ Coating and $Ti_{0.5}Al_{0.4}Si_{0.1}N$ Coating. *Vacuum* **2012**, *86*, 1795–1799. [CrossRef]
21. Chen, L.; Yang, B.; Xu, Y.; Pei, F.; Zhou, L.; Du, Y. Improved Thermal Stability and Oxidation Resistance of Al–Ti–N Coating by Si Addition. *Thin Solid Films* **2014**, *556*, 369–375. [CrossRef]
22. Liew, W.Y.H.; Lim, H.P.; Melvin, G.J.H.; Dayou, J.; Jiang, Z.-T. Thermal Stability, Mechanical Properties, and Tribological Performance of TiAlXN Coatings: Understanding the Effects of Alloying Additions. *J. Mater. Res. Technol.* **2022**, *17*, 961–1012. [CrossRef]
23. Veprek, S.; Männling, H.-D.; Jilek, M.; Holubar, P. Avoiding the High-Temperature Decomposition and Softening of $(Al_{1-x}Ti_x)N$ Coatings by the Formation of Stable Superhard nc-$(Al_{1-x}Ti_x)N$/a-Si_3N_4 Nanocomposite. *Mater. Sci. Eng. A* **2004**, *366*, 202–205. [CrossRef]
24. Veprek, S.; Zhang, R.F.; Veprek-Heijman, M.G.J.; Sheng, S.H.; Argon, A.S. Superhard Nanocomposites: Origin of Hardness Enhancement, Properties and Applications. *Surf. Coat. Technol.* **2010**, *204*, 1898–1906. [CrossRef]
25. Dmitriev, A.I.; Nikonov, A.Y.; Österle, W. MD Sliding Simulations of Amorphous Tribofilms Consisting of either SiO_2 or Carbon. *Lubricants* **2016**, *4*, 24. [CrossRef]
26. Wang, Q.; Zhou, F. Progress in Tribological Properties of Nano-Composite Hard Coatings under Water Lubrication. *Lubricants* **2017**, *5*, 5. [CrossRef]
27. Pfeiler, M.; Zechner, J.; Penoy, M.; Michotte, C.; Mitterer, C.; Kathrein, M. Improved Oxidation Resistance of TiAlN Coatings by Doping with Si or B. *Surf. Coat. Technol.* **2009**, *203*, 3104–3110. [CrossRef]
28. Chang, Y.-Y.; Yang, S.-M. High Temperature Oxidation Behavior of Multicomponent TiAlSiN Coatings. *Thin Solid Films* **2010**, *518*, S34–S37. [CrossRef]
29. Liu, Z.R.; Pei, F.; Chen, L.; Mayrhofer, P.H. Effect of Si-Addition on Structure and Thermal Stability of Ti-Al-N Coatings. *J. Alloys Compd.* **2022**, *917*, 165483. [CrossRef]
30. Sui, X.; Li, G.; Qin, X.; Yu, H.; Zhou, X.; Wang, K.; Wang, Q. Relationship of Microstructure, Mechanical Properties and Titanium Cutting Performance of TiAlN/TiAlSiN Composite Coated Tool. *Ceram. Int.* **2016**, *42*, 7524–7532. [CrossRef]
31. Li, G.; Li, L.; Han, M.; Luo, S.; Jin, J.; Wang, L.; Gu, J.; Miao, H. The Performance of TiAlSiN Coated Cemented Carbide Tools Enhanced by Inserting Ti Interlayers. *Metals* **2019**, *9*, 918. [CrossRef]
32. Gu, J.; Li, L.; Ai, M.; Xu, Y.; Xu, Y.; Li, G.; Deng, D.; Peng, H.; Luo, S.; Zhang, P. Improvement of Solid Particle Erosion and Corrosion Resistance Using TiAlSiN/Cr Multilayer Coatings. *Surf. Coat. Technol.* **2020**, *402*, 126270. [CrossRef]
33. Derflinger, V.H.; Schütze, A.; Ante, M. Mechanical and Structural Properties of Various Alloyed TiAlN-based Hard Coatings. *Surf. Coat. Technol.* **2006**, *200*, 4693–4700. [CrossRef]
34. Chen, L.; Wang, S.Q.; Du, Y.; Zhou, S.Z.; Gang, T.; Fen, J.C.; Chang, K.K.; Li, Y.W.; Xiong, X. Machining Performance of Ti–Al–Si–N Coated Inserts. *Surf. Coat. Technol.* **2010**, *205*, 582–586. [CrossRef]
35. Lü, W.; Li, G.; Zhou, Y.; Liu, S.; Wang, K.; Wang, Q. Effect of High Hardness and Adhesion of Gradient TiAlSiN Coating on Cutting Performance of Titanium Alloy. *J. Alloys Compd.* **2020**, *820*, 153137. [CrossRef]
36. Kot, M.; Rakowski, W.; Major, Ł.; Lackner, J. Load-Bearing Capacity of Coating–Substrate Systems Obtained from Spherical Indentation Tests. *Mater. Des.* **2013**, *46*, 751–757. [CrossRef]
37. Estupiñan, F.A.; Moreno, C.M.; Olaya, J.J.; Ardila, L.C. Wear Resistance of TiAlCrSiN Coatings Deposited by Means of the Co-Sputtering Technique. *Lubricants* **2021**, *9*, 64. [CrossRef]
38. Mikula, M.; Truchlý, M.; Sangiovanni, D.G.; Plašienka, D.; Roch, T.; Gregor, M.; Ďurina, P.; Janík, M.; Kúš, P. Experimental and Computational Studies on Toughness Enhancement in Ti-Al-Ta-N Quaternaries. *J. Vac. Sci. Technol. A* **2017**, *35*, 060602. [CrossRef]
39. Seidl, W.M.; Bartosik, M.; Kolozsvári, S.; Bolvardi, H.; Mayrhofer, P.H. Influence of Ta on the Fracture Toughness of Arc Evaporated Ti-Al-N. *Vacuum* **2018**, *150*, 24–28. [CrossRef]

40. Shugurov, A.R.; Kuzminov, E.D.; Kasterov, A.M.; Panin, A.V.; Dmitriev, A.I. Tuning of Mechanical Properties of $Ti_{1-x}Al_xN$ Coatings through Ta Alloying. *Surf. Coat. Technol.* **2020**, *382*, 125219. [CrossRef]
41. Eremeev, S.V.; Shugurov, A.R. Chemical Bonding Analysis in $Ti_{1-x-y}Al_xTa_yN$ Solid Solutions. *Surf. Coat. Technol.* **2020**, *395*, 125802. [CrossRef]
42. Rachbauer, R.; Holec, D.; Mayrhofer, P.H. Increased thermal stability of Ti–Al–N thin films by Ta alloying. *Surf. Coat. Technol.* **2012**, *211*, 98–103. [CrossRef]
43. Hollerweger, R.; Riedl, H.; Paulitsch, J.; Arndt, M.; Rachbauer, R.; Polcik, P.; Primig, S.; Mayrhofer, P.H. Origin of high temperature oxidation resistance of Ti–Al–Ta–N coatings. *Surf. Coat. Technol.* **2014**, *257*, 78–86. [CrossRef]
44. Shugurov, A.R.; Panin, A.V.; Kasterov, A.M. Effect of Ta alloying on isothermal oxidation behavior of DC magnetron sputtered Ti1-xAlxN coatings on titanium substrate. *Surf. Coat. Technol.* **2021**, *421*, 127488. [CrossRef]
45. Shugurov, A.; Kuzminov, E. Effect of Ta Content on Scratching Behavior of Ti-Al-Ta-N Coatings on Titanium Substrate. *Metals* **2022**, *12*, 1017. [CrossRef]
46. Xian, G.; Zhao, H.-B.; Fan, H.-Y.; Du, H. Structure and Mechanical Properties of Zr/TiAlN Films Prepared by Plasma-Enhanced Magnetron Sputtering. *Rare Met.* **2015**, *34*, 717–724. [CrossRef]
47. Stoney, G.G.; Parsons, C.A. The Tension of Metallic Films Deposited by Electrolysis. *Proc. R. Soc. Lond. A* **1909**, *82*, 172–175. [CrossRef]
48. Oliver, W.C.; Pharr, G.M. An Improved Technique for Determining Hardness and Elastic Modulus Using Load and Displacement Sensing Indentation Experiments. *J. Mater. Res.* **1992**, *7*, 1564–1583. [CrossRef]
49. Tanaka, Y.; Ichimiya, N.; Onishi, Y.; Yamada, Y. Structure and Properties of Al–Ti–Si–N Coatings Prepared by the Cathodic Arc Ion Plating Method for High Speed Cutting Applications. *Surf. Coat. Technol.* **2001**, *146*, 215–221. [CrossRef]
50. Hsu, T.-W.; Greczynski, G.; Boyd, R.; Kolozsvári, S.; Polcik, P.; Bolz, S.; Bakhit, B.; Odén, M. Influence of Si Content on Phase Stability and Mechanical Properties of TiAlSiN Films Grown by AlSi-HiPIMS/Ti-DCMS Co-Sputtering. *Surf. Coat. Technol.* **2021**, *427*, 127661. [CrossRef]
51. Scherrer, P. *Bestimmung Der Inneren Struktur Und Der Größe von Kolloidteilchen Mittels Röntgenstrahlen. Kolloidchemie Ein Lehrbuch*; Zsigmondy, R., Ed.; Springer: Berlin/Heidelberg, Germany, 1912; pp. 387–409; ISBN 978-3-662-33915-2.
52. Pelleg, J.; Zevin, L.Z.; Lungo, S.; Croitoru, N. Reactive-Sputter-Deposited TiN Films on Glass Substrates. *Thin Solid Films* **1991**, *197*, 117–128. [CrossRef]
53. Xu, Z.; Zhang, Z.; Bartosik, M.; Zhang, Y.; Mayrhofer, P.H.; He, Y. Insight into the Structural Evolution during TiN Film Growth via Atomic Resolution TEM. *J. Alloys Compd.* **2018**, *754*, 257–267. [CrossRef]
54. Karlsson, L.; Hultman, L.; Sundgren, J.-E. Influence of Residual Stresses on the Mechanical Properties of TiC_xN_{1-x} (x = 0, 0.15, 0.45) Thin Films Deposited by Arc Evaporation. *Thin Solid Films* **2000**, *371*, 167–177. [CrossRef]
55. Mayrhofer, P.H.; Kunc, F.; Musil, J.; Mitterer, C. A Comparative Study on Reactive and Non-Reactive Unbalanced Magnetron Sputter Deposition of TiN Coatings. *Thin Solid Films* **2002**, *415*, 151–159. [CrossRef]
56. Leyland, A.; Matthews, A. On the Significance of the H/E Ratio in Wear Control: A Nanocomposite Coating Approach to Optimised Tribological Behaviour. *Wear* **2000**, *246*, 1–11. [CrossRef]
57. Tsui, T.Y.; Pharr, G.M.; Oliver, W.C.; Bhatia, C.S.; White, R.L.; Anders, S.; Anders, A.; Brown, I.G. Nanoindentation and Nanoscratching of Hard Carbon Coatings for Magnetic Disks. Mater. *Res. Soc. Symp. Proc.* **1995**, *383*, 447–452. [CrossRef]
58. Musil, J. Hard Nanocomposite Coatings: Thermal Stability, Oxidation Resistance and Toughness. *Surf. Coat. Technol.* **2012**, *207*, 50–65. [CrossRef]
59. Bull, S.J. Failure Modes in Scratch Adhesion Testing. *Surf. Coat. Technol.* **1991**, *50*, 25–32. [CrossRef]
60. Favache, A.; Sacré, C.-H.; Coulombier, M.; Libralesso, L.; Guaino, P.; Raskin, J.-P.; Bailly, C.; Nysten, B.; Pardoen, T. Fracture Mechanics Based Analysis of the Scratch Resistance of Thin Brittle Coatings on a Soft Interlayer. *Wear* **2015**, *330*, 461–468. [CrossRef]
61. Hutchinson, J.W.; Suo, Z. Mixed Mode Cracking in Layered Materials. *Adv. Appl. Mech.* **1991**, *29*, 63–191. [CrossRef]
62. Evans, A.G.; He, M.Y.; Hutchinson, J.W. Effect of Interface Undulations on the Thermal Fatigue of Thin Films and Scales on Metal Substrates. *Acta Mater.* **1997**, *45*, 3543–3554. [CrossRef]
63. Strawbridge, A.; Evans, H.E.; Ponton, C.B. Spallation of Oxide Scales from NiCrAlY Overlay Coatings. *Mater. Sci. Forum* **1997**, *251*, 365–372. [CrossRef]